NWP SAF

Satellite Application Facility
for Numerical Weather Prediction

Document No. NWPSAF–EC–TR–006

Version 1.0

May 10, 2004

Microwave radiative transfer modeling in clouds and precipitation
Part II: Model evaluation

Emmanuel Moreau, Peter Bauer, Frédéric Chevallier

European Centre for Medium–Range Weather Forecasts

Microwave radiative transfer modeling in clouds and precipitation

Part II: Model evaluation

Emmanuel Moreau, Peter Bauer, Frédéric Chevallier

ECMWF

This documentation was developed within the context of the EUMETSAT satellite Application Facility on Numerical Weather Prediction (NWP SAF), under the Cooperation Agreement dated 25 November 1998, between EUMETSAT and the Met Office, UK, by one or more partners within the NWP SAF. The partners in the NWP SAF are the Met Office, ECMWF, KNMI and Météo France.

Change record			
Version	Date	Author / changed by	Remarks

Contents

1 Introduction **3**

2 Eddington vs. Doubling–Adding model **4**

2.1 Model profiles 4

2.2 Sub–grid variability 4

2.3 Results 6

2.4 Computing time 7

3 Comparison with other models **7**

3.1 Input data 8

3.2 Results 9

Abstract

An evaluation of those models which were introduced in part I of this report was carried out. Based on ECMWF model cloud and precipitation profiles a relative comparison of doubling–adding and Eddington models revealed that apart from situations with excessive amounts of snow (snow paths $>1 kg\,m^{-2}$) both models agree within radiometer noise level, i.e., within 0.5 K. The treatment of sub–gridscale cloud variability was identified as an important source of error. At frequencies above 37 GHz, a separation of the average cloud profile into three sub–profiles, namely cloudfree, ice and water cloud portions with corresponding maximum fractional coverage, seemed favorable. An intercomparison with radiative transfer codes from independent research groups also revealed the good performance of the two models. In conclusion, the Eddington model showed acceptable accuracy with a 30 times higher computational efficiency thus being well suited for global application at microwave frequencies <100 GHz.

1 Introduction

In part I (Bauer 2002), the principles of microwave radiative transfer were introduced along with two simulation models, namely the Matrix–Operator or Doubling–Adding model (DA) and the Eddington approximation (EDD). DA can be considered accurate due to the explicit computation of multiple scattering through combination of optically thin layers. By increasing the number of discrete angles the accuracy of this model can be further refined because stronger scattering in the presence of larger particles will produce more complex scattering phase functions which requires a dense sampling. The approximation in EDD eliminates the need for an explicit phase function and reduces the number of discrete angles to that of the observation. With the addition of a δ–function in case of highly asymmetric phase functions, this method has been widely applied to all sorts of problems in atmospheric transfer with sufficient accuracy. Both radiative transfer models only assume plane–parallel atmospheres.

In part II, the treatment of sub–gridscale cloud variability is introduced. The two models are then compared to each other and eventually compared with some independent models. Since the objective is to provide models to be implemented in global model environments (e.g. for data assimilation or model validation), the first comparison was carried out using model profiles of the current ECMWF forecast model. The comparison with other models originates from an effort initiated during precipitation retrieval method (using passive microwave satellite data) evaluation projects in which the question in how far the forward modeling contributes to total errors became an issue.

2 Eddington vs. Doubling–Adding model

2.1 Model profiles

An intercomparison between two radiative transfer models (Bauer 2002) was performed using ECMWF model CY23R4 ($T_L511L60$) fields as an input. Profiles of temperature, specific humidity, cloud liquid water, solid and liquid precipitation rates and surface parameters such as surface pressure, skin temperature, and surface wind speed were generated from 6–hour forecasts at 00, 06, 12 and 18 UTC on January 1, 2001. This dataset contained 55,174 cases. The frequency of occurrence of some of the above parameters as well as the data coverage by latitude is displayed in Figure 1. For all situations, radiances at the top of the atmosphere were simulated using both models at frequencies of 10.65, 19.35, 22.235, 37.0, and 85.5 GHz and at vertical and horizontal polarization for various incidence angles between 0 (nadir) and 65 degrees. Surface emissivity and reflectivity were calculated with the fast emissivity model FASTEM–2 (English and Hewison 1998) while atmospheric absorption was computed from the line–by–line model of Liebe et al. (1992). The investigated frequencies correspond to those available from the Special Sensor Microwave / Imager (SSM/I; Hollinger et al. 1990) and Tropical Rainfall Measuring Mission (TRMM) Microwave Imager (TMI; Kummerow et al. 1998) radiometers.

2.2 Sub–grid variability

With the resolution of current global models, the effect of sub–gridscale variability of clouds and precipitation will have a strong impact on gridscale averaged brightness temperatures. Since the brightness temperature–rainrate (or other cloud parameter) relationship is non–linear the averaged brightness temperatures (TB) from sub–profiles will differ from the TB of the averaged profile. The geometry of the hydrometeor profiles in the forecast scheme is rather complex. Indeed, fractional cloud cover and fractional precipitation cover are defined separately in each atmospheric layer. The cloud layers are overlapped following a maximum–random approximation. Precipitation is distributed in the vertical in consistence with the corresponding cloud geometry and the model physics and a distinction is made between stratiform (large–scale) and convective precipitation.

This complex geometry may be correctly accounted for within complex 3–dimensional Monte–Carlo models. Since the computational burden of scattering calculations represents a limiting factor for application to large number of profiles, as is done in global model environments, simplifications to the hydrometeor structure need to be done. Microwave radiation is sensitive to large amounts of hydrometeors only so that rather simple box–type geometries may serve as a first–order approximation. Two hypotheses are introduced:

1. a sub–division into cloud covered and cloudfree part (= 2Box) where the cloud and precipitation fractions equal the maximum occurring water or ice cloud fraction along the profile;

2. a sub–division into a cloudfree part, a common part of liquid and ice cloud water and precipitation, and a column containing the excess ice/snow (for ice/snow coverage > cloud/rain coverage) or vice versa (=3Box).

The radiative transfer model was applied independently to the sub–profiles and the final TB's were then calculated from the sum of the two/three TB's weighted by the corresponding cloud fraction.

Both options are identical if maximum ice and water cloud fractions are identical. This occurs in 32% of the above introduced sample. Figure 2 illustrates the corresponding frequency distributions indicating that apart from full coverage for widespread large–scale precipitation, liquid clouds tend to have a maximum near cloud fraction 0.4–0.5 while ice clouds mainly occur in convection with smaller fractions. Therefore significant differences can be expected between 2Box and 3Box treatments where convection dominates.

TB's for both assumptions were calculated with the EDD model and for the 7 SSM/I channels. Table 1 and Figure 3 summarize the results. For the three lower channels, systematic differences tend to be negligible with standard deviations well below 0.4 K. At 37.0 and 85.5 GHz, problems occur when scattering is strong enough so that the difference between ice and water cloud fractions becomes effective, i.e., the third sub–profile contributes significantly to the average TB's. At 37.0 GHz the 2Box simulations generally produce smaller TB's than those from the 3Box simulations. At 85.5 GHz and for very strong scattering this behavior is reversed.

The two regimes obviously originate from situations where 2Box overestimates scattering (maximum ice cloud fraction larger than maximum water cloud fraction) or underestimates scattering (maximum ice cloud fraction smaller than maximum water cloud fraction). Figure 2 suggests this separation through the relative displacement between the two bi–modal distributions. While for the relative intercomparison of the two models the implementation of the 2Box model seemed sufficient the differences were considered significant enough to implement the 3Box assumption for future calculations.

Table 1: 3Box–2Box difference statistics for SSM/I channels (in K; v/h refer to polarization).

Channels	19.35 (v)	19.35 (h)	22.235 (v)	37.0 (v)	37.0 (h)	85.5 (v)	85.5 (h)
Mean deviation	0.04	0.04	0.04	0.23	0.49	-0.38	0.08
Standard deviation	0.25	0.34	0.25	0.60	1.35	2.46	1.84

In the absence of rain, the hypothesis on cloud cover (i.e. maximally overlapped cloud layers with a unique cover in the vertical) may be compared with a more elaborate cloud layer overlap hypothesis. As an illustration, Figure 4 shows the difference between the 37.0 GHz TB's with horizontal polarization computed with a simple 2Box–model with those using the maximum–random overlap hypothesis (Räisänen 1998). The main impact of the simplification appears for the highest TB's which are underestimated by a 2–3 K by the 2Box model. This

effect can be explained by the overestimated cloud extent by the 2Box model since it adjusts all cloud layer fractions to that of the maximum.

2.3 Results

The major sources of differences between the doubling–adding model (DA) and the δ-Eddington model (EDD) are the treatment of:

1. (multiple) scattering in the atmosphere: For DA, the Henyey–Greenstein phase function describes the distribution of single scattered radiation with scattering angle. Multiple scattering is explicitly treated for discrete angles. In EDD, the phase function is approximated by a first–order series and multiple scattering is implicitly treated through flux continuity at layer boundaries. Since in EDD only the asymmetry parameter provides information on phase function shape, more complex angular scattering patterns are not represented.

2. radiation interaction with the surface: DA treats the surface like an atmospheric layer while EDD uses the hemispherically averaged emissivity for the boundary conditions and a single specular emissivity for combining atmosphere and surface contributions. Therefore, the variation of emissivity with angle is less well represented in EDD.

Figure 5 summarizes the systematic and random differences between both models at 10.65, 19.35, 22.235, 37.0, and 85.5 GHz and both polarizations from simulations of the above described data.

In case of little atmospheric scattering, i.e., at frequencies below 22.235 GHz, the two models produce almost identical results with maximum systematic differences (ΔTB) below 0.15 K and maximum random differences below 0.2 K. The increase of differences between brightness temperatures with incidence angle results from the increase in optical path (more multiple scattering) and the stronger gradient of emissivity. Both will modify DA–TB's to a stronger extent than EDD–TB's. The difference between vertical and horizontal polarizations only originates from surface emission/reflection (see part I). At 37.0 and 85.5 GHz, the differences increase slightly but remain below 0.5 K for incidence angles below 55 degrees.

The global statistics represented in Figure 5 were further stratified to isolate contributions from scattering in the atmosphere and surface emission/reflection. First, all simulations were repeated with constant emissivities, i.e. at each incidence angle the corresponding emissivity was taken for all other angles (see Figure 6). Since only DA allows for cross–talk between polarizations, the remaining polarization difference originates from DA that is the contribution of horizontally polarized emissivities to vertically polarized TB's and vice versa. Since there is only little overall difference between Figure 5 and Figure 6 the latter explains most of the variation of ΔTB with angle. The most important requirement for the surface emissivity model is therefore the reproduction of an accurate emissivity at the observation angle and at both polarizations.

In Figures 7 and 8, the simulations are plotted against integrated snow water content since snow represents the strongest source of scattering in the atmosphere. Already from Figure 1 it could be observed that unrealistically large snow paths occur, sometimes with only little liquid precipitation. As expected, ΔTB generally increases with snow water path and frequency, thus multiple scattering accounts for most of the model differences. At an incidence angle of 54 degrees the scattering sensitivity shifts towards lower snow contents due to the optical path which increases by $1/cos(54^o)$ ($\approx$1.7). In clear skies (snow water path = 0 $kg\,m^{-2}$) no scattering occurs and thus $\Delta TB = 0$.

In summary, systematic differences/standard deviations between DA and EDD model simulations were found to remain below 0.1/0.1, 0.5/0.3, 0.4/0.5, 0.9/1.0, and -1.2/1.6 K at 10.65, 19.35, 22.235, 37.0, and 85.5 GHz, respectively. The different treatment of multiple scattering explains the bulk of these differences since for snow water paths below 1 $kg\,m^{-2}$, the models produce TB's which agree within limits of current radiometer noise ($\approx$0.5 K). An important ingredient is the usage of an accurate surface emissivity model and a proper treatment of fractional cloud coverage within the simulated grid box.

2.4 Computing time

Since the above models aim at the computation of radiances at multiple frequencies and polarizations within an operational global modeling framework, computing time is a major issue. Table 2 shows an assessment of computing time after application of both DA and EDD models to 100 rain affected model atmospheres and to 7 microwave (SSM/I) frequencies. Independent of the level of optimization, which has only a little impact on the CPU times, the DA–model is about 30 times slower than the EDD–model of which most is spent on the averaging of the phase function. Here, pre–calculated tables may offer an alternative. However, given the high level of accuracy of EDD, its computational efficiency is by far more adequate for its use within an assimilation system.

Table 2: CPU time in seconds (SGI Origin 2000) for the simulation of seven SSM/I channels in 100 rain affected model profiles.

Optimization level	Eddington model	Doubling Adding model
-O2	11.3	298.1
-O3	10.4	240.4

3 Comparison with other models

An intercomparison of the above models with independent microwave multiple scattering radiative transfer code is included here for the sake of completeness. More details of this intercomparison can be found in Smith et al. (2002). The intercomparison was organized

Table 3: Specification of model features.

Model	Reference	Specifications	Surface
1: CU	Evans and Stephens (1990)	two–stream Eddington	Fresnel
2: CU	Evans and Stephens (1990)	two–stream Eddington, δ–scaling	Fresnel
3: FSU	Mugnai and Smith (1988)	two–stream Sobolev, δ–scaling	Fresnel
4: FSU	Mugnai and Smith (1988)	two–stream Sobolev, δ–scaling	Lambertian
5: IFA	Marzano et al. (1994)	16–stream discrete ordinate	Lambertian
6: NASA	Kummerow (1993)	two–stream Eddington	Fresnel
7: NASA	Roberti et al. (1994)	reverse Monte Carlo	Fresnel
8: ECMWF	Bauer et al. (1998)	two–stream Eddington (EDD)	Fresnel
9: ECMWF	Bauer and Schlüssel (1993)	matrix operator (DA)	Fresnel

in the framework of rainfall retrieval algorithm developments aiming at the quantification of radiative transfer model uncertainties as a source of rainfall retrieval errors.

A set of profiles containing liquid water and ice contents of cloud and rain water as well as snow, graupel, and pristine ice were distributed to the participants together with a black box routine providing Mie single scattering, atmospheric background absorption, and surface emissivity. Simulations were to be carried out for nadir and off–nadir (53.1^o) observation angles at frequencies between 10 and 85 GHz. Among the radiative transfer models were two–stream, multiple stream, and Monte Carlo models (see Table 3 for details).

3.1 Input data

The directions and constants needed for making the calculations were specified as follows:

- Microwave frequencies for output at 10.7, 19.4, 37.0, 85.5 GHz, satellite zenith angles of 53.1 degrees and 0.0 degrees corresponding to the spaceborne Special Sensor Microwave / Imager (SSM/I) and the airborne Advanced Microwave Precipitation Radiometer (AMPR), respectively. Surface temperature of 300 K, surface emissivities of 0.85 for land and 0.4 for ocean, and cosmic background temperature of 2.7 K were prescribed.

- All calculations were to be polarization independent, that is also for Fresnel reflection the polarization of incident unpolarized radiation was neglected.

- Four profiles were provided, representing four configurations of cloud states: (1) low water, low ice content (associated rainrate of 0.94 mm/hr), (2) low water, high ice content (associated rainrate of 0.34 mm/hr), (3) high water, low ice content (associated rainrate of 9.46 mm/hr), (4) high water, high ice content (associated rainrate of 90.23 mm/hr).

- Profile information served as input to a Mie "black box" which generated volume extinction and scattering coefficients as well as asymmetry factors, plus total volume extinction

and scattering coefficients (km^{-1}), total asymmetry factor, and combined gaseous absorption coefficients for oxygen and water (km^{-1}) given for 41 layers. The latter were obtained from the Millimeter Propagation Model (MPM) of Liebe et al. (1992). For those models requiring phase functions, the Henyey–Greenstein approximation was prescribed to be obtained from the asymmetry factors.

The profiles had been selected from a mesoscale non–hydrostatic cloud model simulation of a continental storm system during the Cooperative Huntsville Meteorological Experiment in 1986. The profiles had 42 levels, the lowest level corresponding to the surface. At each level, the variables were height, temperature, pressure, specific humidity, vertical velocity, cloud and rain liquid water content as well as graupel, pristine ice crystal, snow, and aggregate ice water contents. For the precipitating species, exponential size distributions were assumed while for cloud droplets and pristine ice crystals were taken to be monodisperse with diameters of 0.01 mm and 0.1 mm, respectively.

Figure 9 displays the input profiles of volume extinction coefficient, k, single scattering albedo, ω_o, and asymmetry parameter, g, at 10.7, 19.4, 37.0, and 85.5 GHz, respectively. At 85.5 GHz, the extinction profile follows the rain liquid water distribution while ω_o indicates nicely the precipitating ice (snow and graupel) concentrations. The total ice amounts of cases 2 and 4 are about the same while case 4 shows multiple maxima.

3.2 Results

Figures 10–11 summarize the results for a zenith angle of 53.1 degrees and both surfaces. For convenience, only the four window frequencies where atmospheric absorption is small compared to hydrometeor contributions are presented. Over land (Figure 10) and between 10.7 and 37.0 GHz, all those models using Fresnel surface reflection produce almost identical results. The assumption of isotropic reflectors increases the upwelling radiances significantly by 1–5 K at 0 degree incidence and <2 K at 53.1 degree incidence. These differences might be partially compensated if parameterizations for rough surfaces are accounted for in Fresnel reflection.

Once scattering in the atmosphere becomes important (at 85.5 GHz, in particular for cases 2 and 4), the influence of the model treatment of multiple scattering overrides the surface effect. Those two–stream models which do not include δ–scaling, i.e., do not account for the more extreme peak of the phase function in forward scattering direction, produce higher TB's. Models 4 and 5 (Lambertian surface) still overestimate TB's with respect to the other models but to a lesser extent than the unscaled models. The difference between multiple–stream and Monte Carlo models (models no. 5, 7, 9 in case 4 at 85.5 GHz) always remains below 1 K where the surface has no effect. At nadir incidence, δ–scaling does not fully compensate the two–stream simplification because δ–scaling is most accurate where the observation angle corresponds to the zero–th order discrete angle in the quadrature formula (see part I).

Over oceans (Figure 11), the lower surface emissivities produce larger differences since both emission and scattering in the atmosphere are detectable in the response of TB's to cloud

condition. The surface emission treatment becomes even more relevant. At nadir incidence, the Lambertian models produce TB's which are 20 K too high. For 53.1 degree incidence, this limit is reduced to 5 K. Again, the multiple–stream and Monte Carlo models are very close for opaque and strongly scattering atmospheres.

In summary of all comparisons, it was found that:

- δ–scaling makes little difference for the SSM/I incidence angle (worst case 0.5 K for land at 85.5 GHz, 0.75 K for ocean), but large difference for nadir incidence (7–8 K at 85.5 GHz, 3 K at 37 GHz).
- Switching from Fresnel to Lambertian boundary conditions at fixed emissivity makes little difference at SSM/I incidence over land, but over 2 K for water at 10.7 GHz; at nadir incidence over land, differences are 3–5 K across all frequencies, while over ocean differences are approximately 20 K over the 10.7–37.0 GHz range.
- Going from two–stream to 16–stream for Lambertian boundary conditions produces worst case differences at 85.5 GHz of around 2.5 K for SSM/I incidence, while at nadir incidence worst case differences at 85.5 GHz are around 1 K over land and 3.5 K over ocean.
- The worst case differences between two–stream and reverse Monte Carlo are 2.5 K at SSM/I incidence, and half that for nadir incidence.
- As would be expected, the differences between 16–stream and reverse Monte Carlo are smaller than the differences between two–stream and reverse Monte Carlo – where these comparisons can be made (only when the upwelling TB's are insensitive to surface boundary conditions since the IFA calculations used a Lambertian surface and the NASA Monte Carlo calculations used a Fresnel surface).

References

Bauer, P. and P. Schlüssel, 1993: Rainfall, total water, ice water and water–vapour over sea from polarized microwave simulations and SSM/I data, *J. Geophys. Res.*, **98**, 20737–20759.

Bauer, P., L. Schanz, and L. Roberti, 1998: Correction of three–dimensional effects for passive microwave retrievals of convective precipitation, *J. Appl. Meteor.*, **37**, 1619–1632.

Bauer, P., 2002: Microwave radiative transfer modeling in clouds and precipitation. Part I: Model description. NWP–SAF report No. 5, available from NWP–SAF hosted by The Met Office, Bracknell UK, 29 pp.

English, S., and T.J. Hewison, 1998: A fast generic millimetre wave emissivity model. In *Proceedings of the International Society for Optical Engineering (SPIE) on Microwave Remote Sensing of the Atmosphere and Environment*, T. Hayasaka, D.L. Wu, Y.–Q. Jin, J.–S. Jiang (Eds.), **3503**, 22–30.

Evans, F.K. and G.L. Stephens, 1990: Polarized microwave radiative transfer modeling: An application to microwave remote sensing of precipitation. Colorado State University, Dept. of Atmos. Sci., Paper No. 461, Fort Collins, CO, pp. 79.

Hollinger, J., J.L. Pierce, and G.A. Poe, 1990: SSM/I instrument evaluation. *IEEE Trans. Geosci. Remote Sens.*, **28**, 781–790.

Kummerow, C., W. Barnes, T. Kozu, J. Shiue, and J. Simpson, 1998: The Tropical Rainfall Measuring Mission (TRMM) sensor package. *J. Atmos. Ocean. Tech.*, **15**, 809–817.

Liebe, H. J., Rosenkranz, P., and G. A. Hufford, 1992: Atmospheric 60 GHz oxygen spectrum: New laboratory measurements and line parameters.*J. Quant. Spec. Rad. Trans.*, **48**, 629–643.

Marzano, F.S., A. Mugnai, E.A. Smith, X. Xiang, J. Turk, and J. Vivekanandan, 1994: Active and passive remote sensing of precipitating storms during CaPE. Part II: Intercomparison of precipitation retrievals from AMPR radiometer and CP-2 radar. *J. Meteor. Atmospheric Physics*, **54**, 29–51.

Mugnai, A. and E.A. Smith, 1988: Radiative transfer to space through a precipitating cloud at multiple microwave frequencies. Part I: Model description. *J. Appl. Meteor.*, **27**, 1055–1073.

Räisänen, P., 1998: Effective longwave cloud fraction and maximum–random overlap of clouds – A problem and a solution. *Mon. Wea. Rev.*, **126**, 3336–3340.

Roberti, L., J. Haferman, and C.D. Kummerow, 1994: Microwave radiative transfer through horizontally inhomogeneous precipitating cloud. *J. Geophys. Res.*, **99**, 16707–16718.

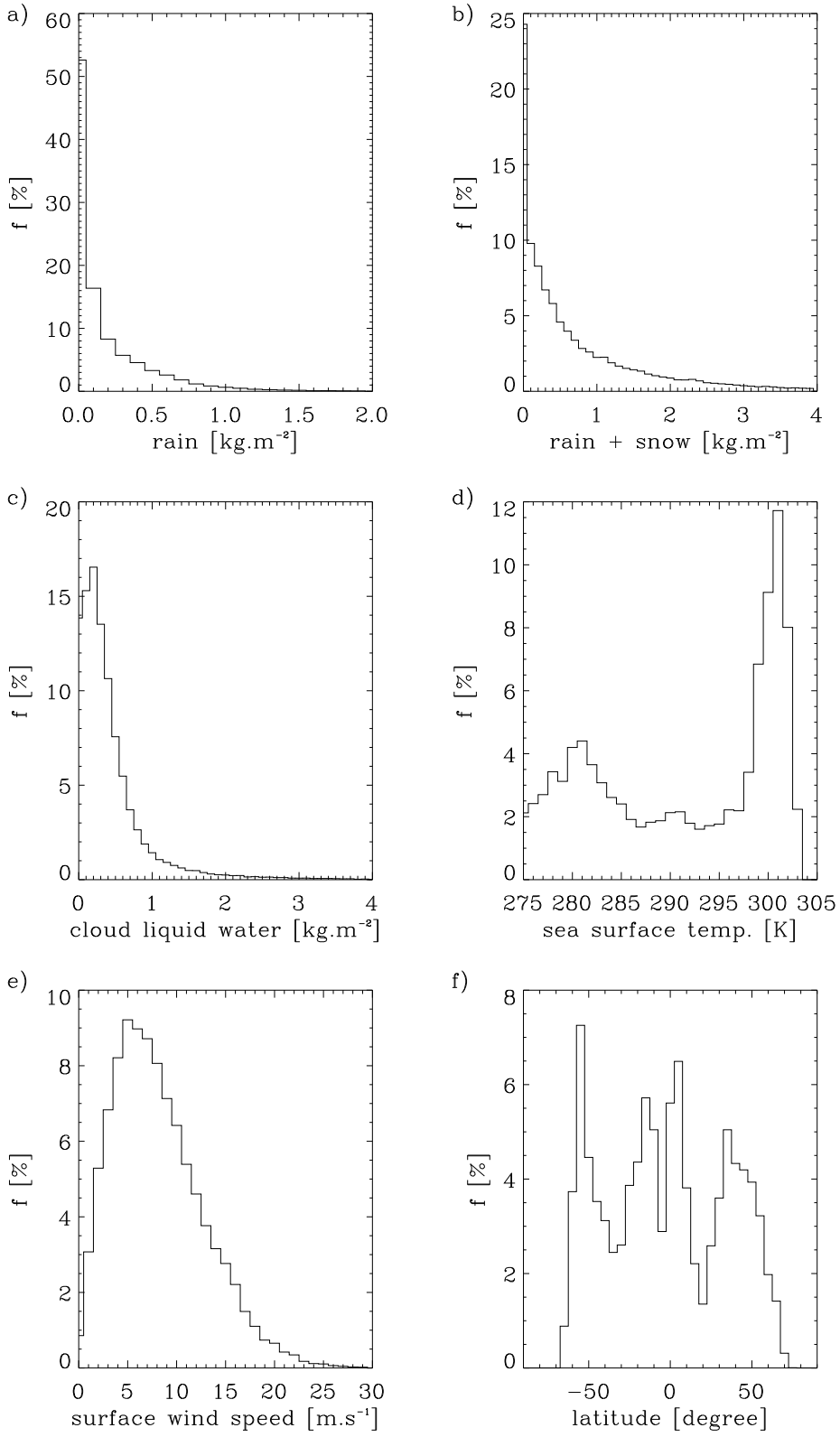

Figure 1: Frequency distributions of rain water path (a), rain+snow water path (b), cloud liquid water path (c), sea surface temperature (d), near–surface windspeed (e), and data coverage by latitude (e).

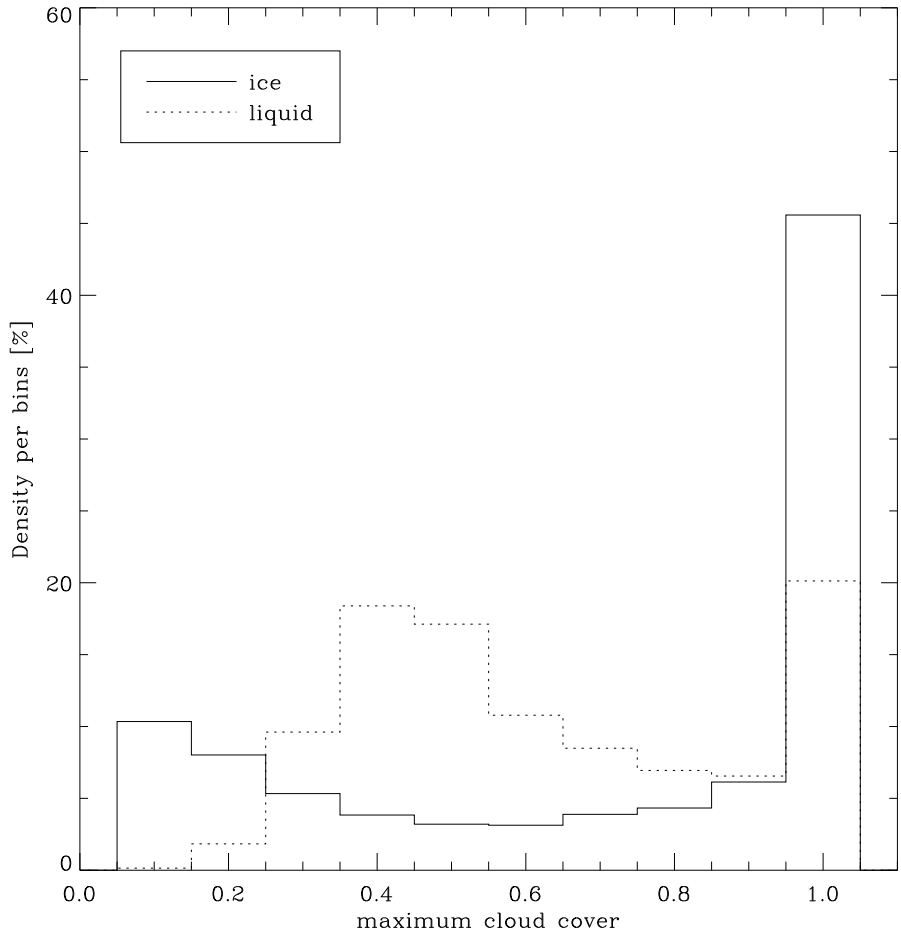

Figure 2: Probability distribution of maximum rain and ice cloud fractions (when they are not identical).

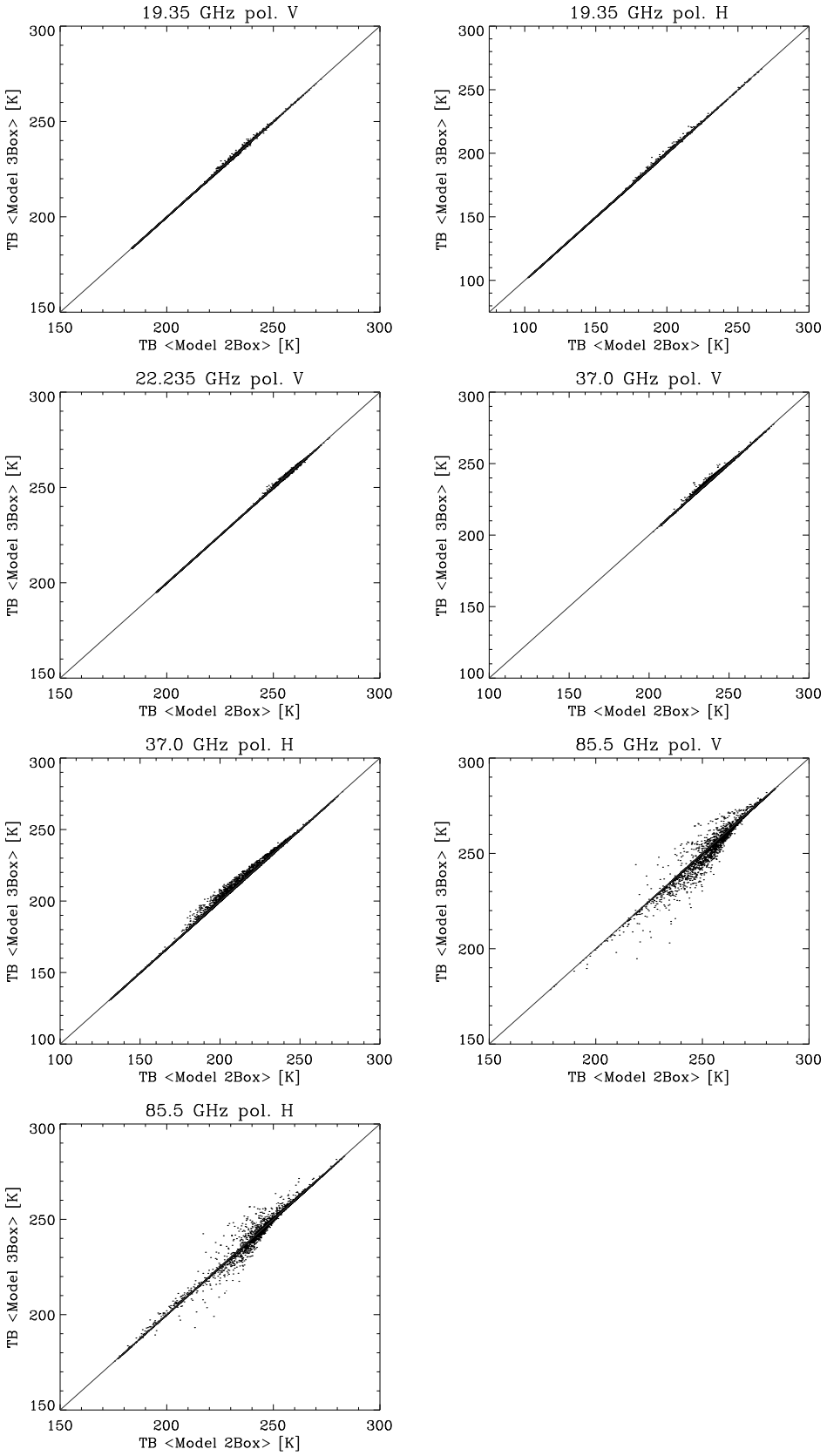

Figure 3: 2Box vs. 3Box TB's at SSM/I frequencies (6,382 samples with rain water path > 0.01 $kg\,m^{-2}$.)

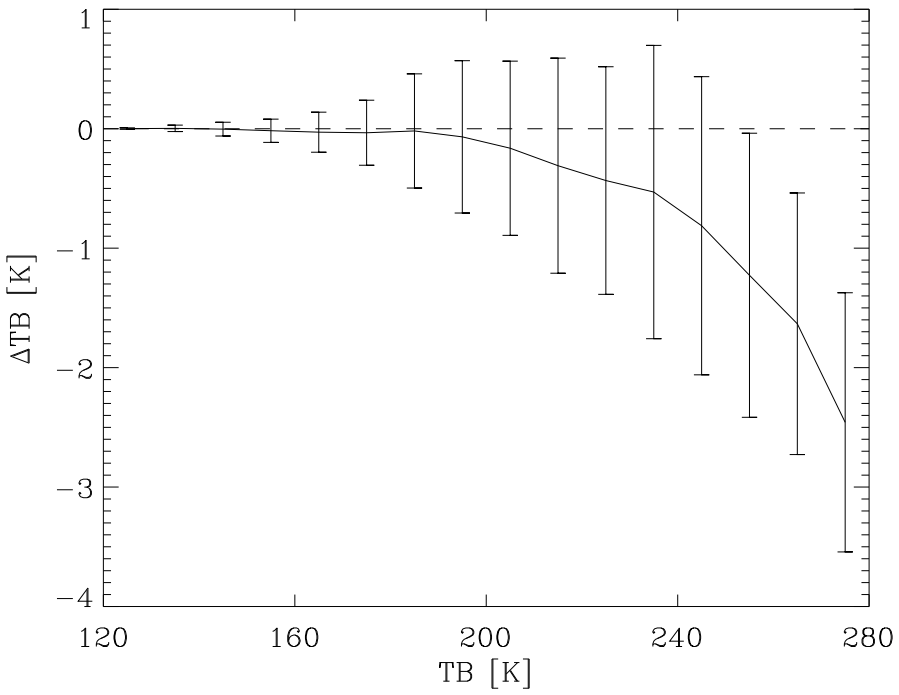

Figure 4: Mean and standard deviation between 37.0 GHz (h) TB's from 2Box and maximum–random overlap cloud profiles for non–precipitating systems.

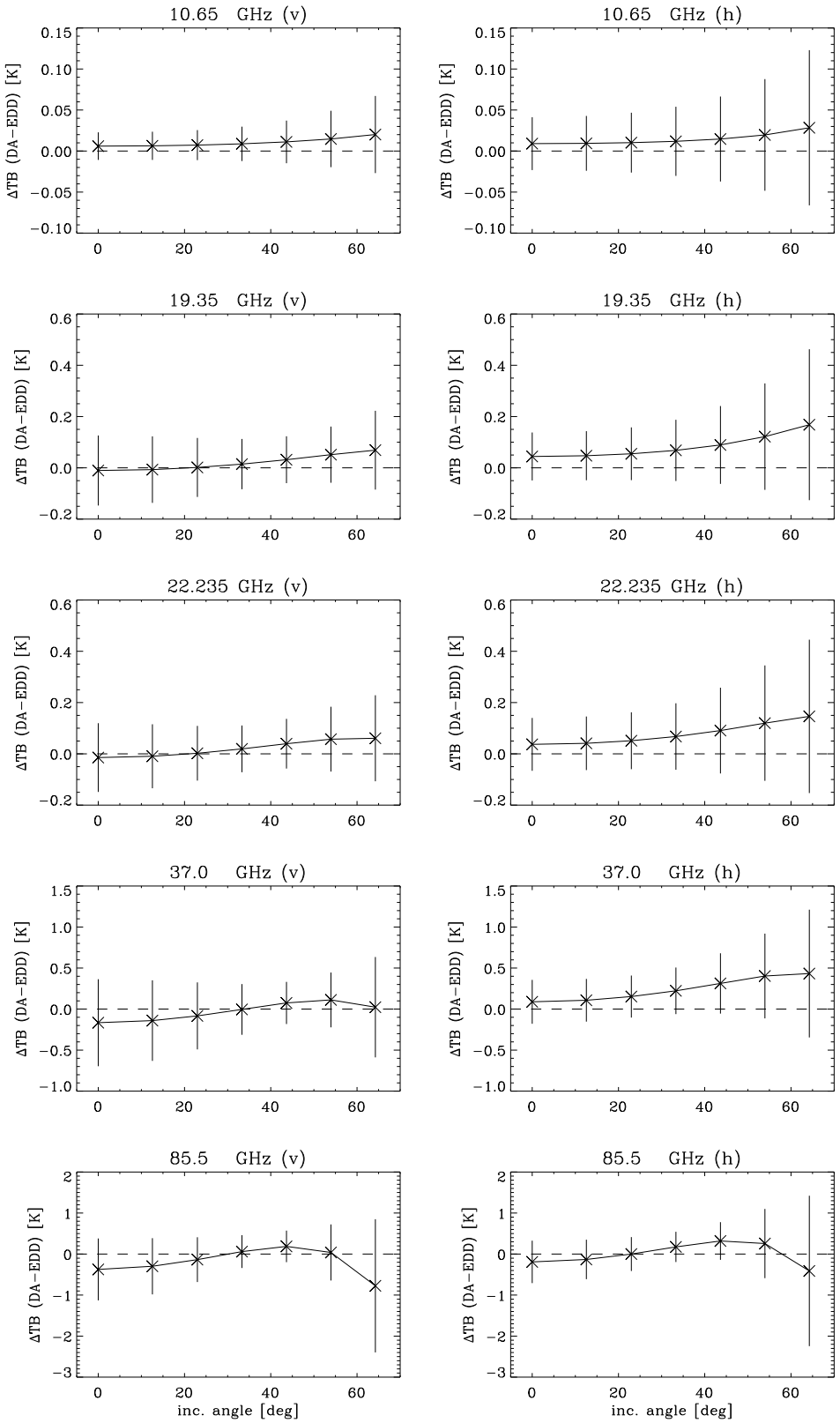

Figure 5: Mean DA–EDD differences at 10.65, 19.35, 22.235, 37.0, and 85.5 GHz (left panels: vertical polarization, right panels: horizontal polarization); error bars correspond to +/− one standard deviation.

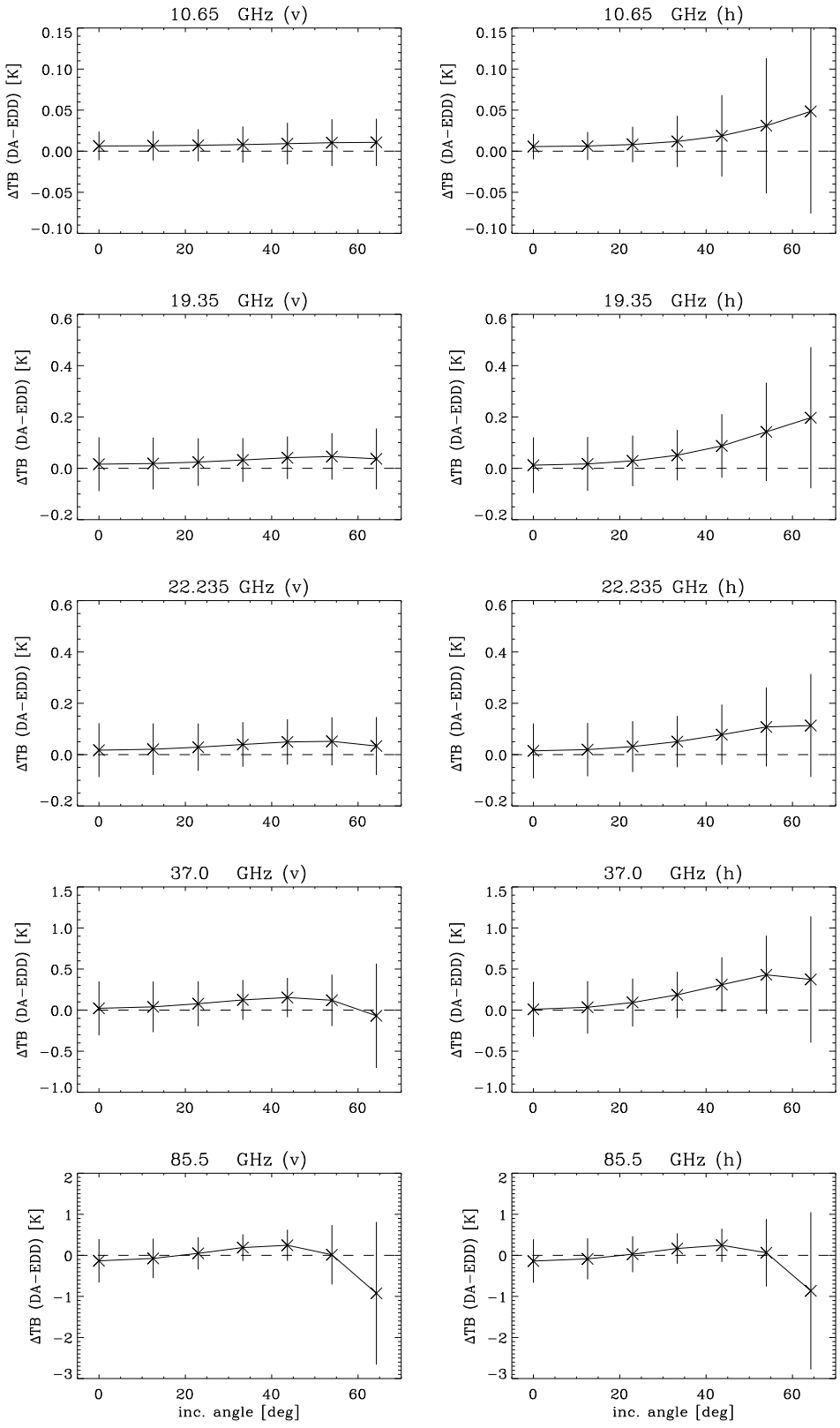

Figure 6: Same as Figure 5 for constant emissivities.

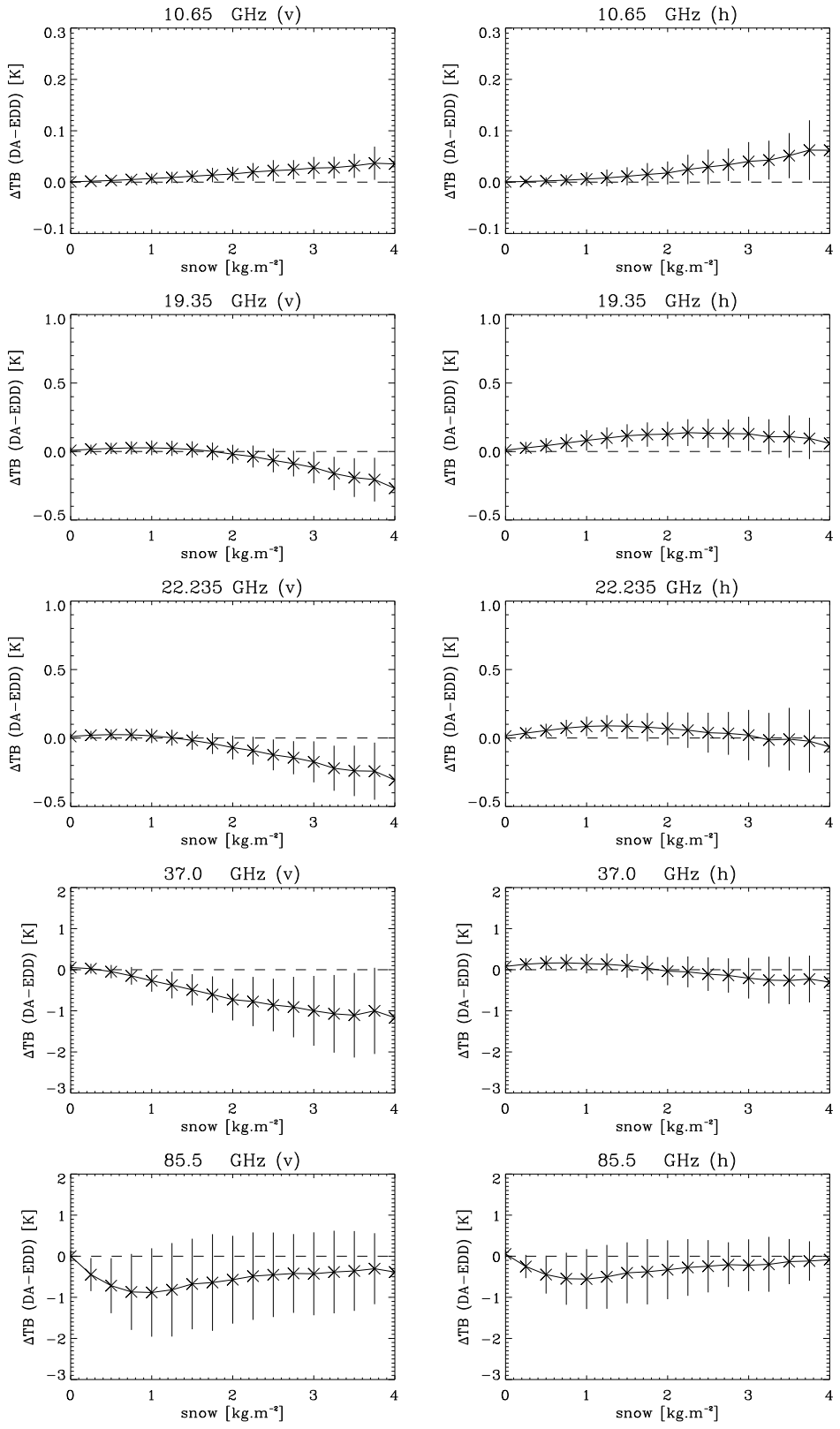

Figure 7: Systematic DA–EDD differences at 10.65, 19.35, 22.235, 37.0, and 85.5 GHz as a function of the integrated snow water path and at nadir incidence angle. The error bar corresponds to +/− one standard deviation.

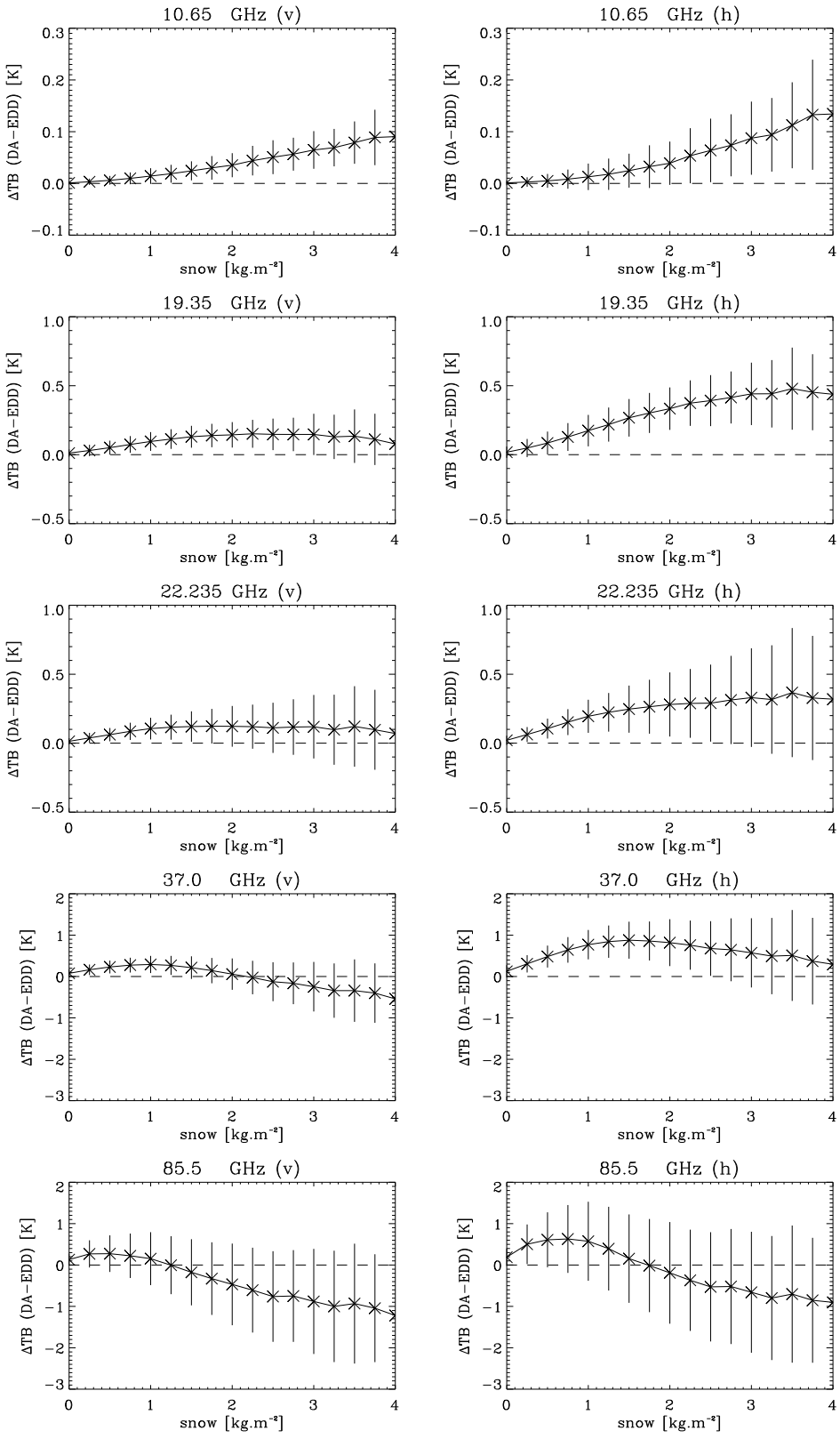

Figure 8: Same as Figure 7 but for an incidence angle of 54.0 degree.

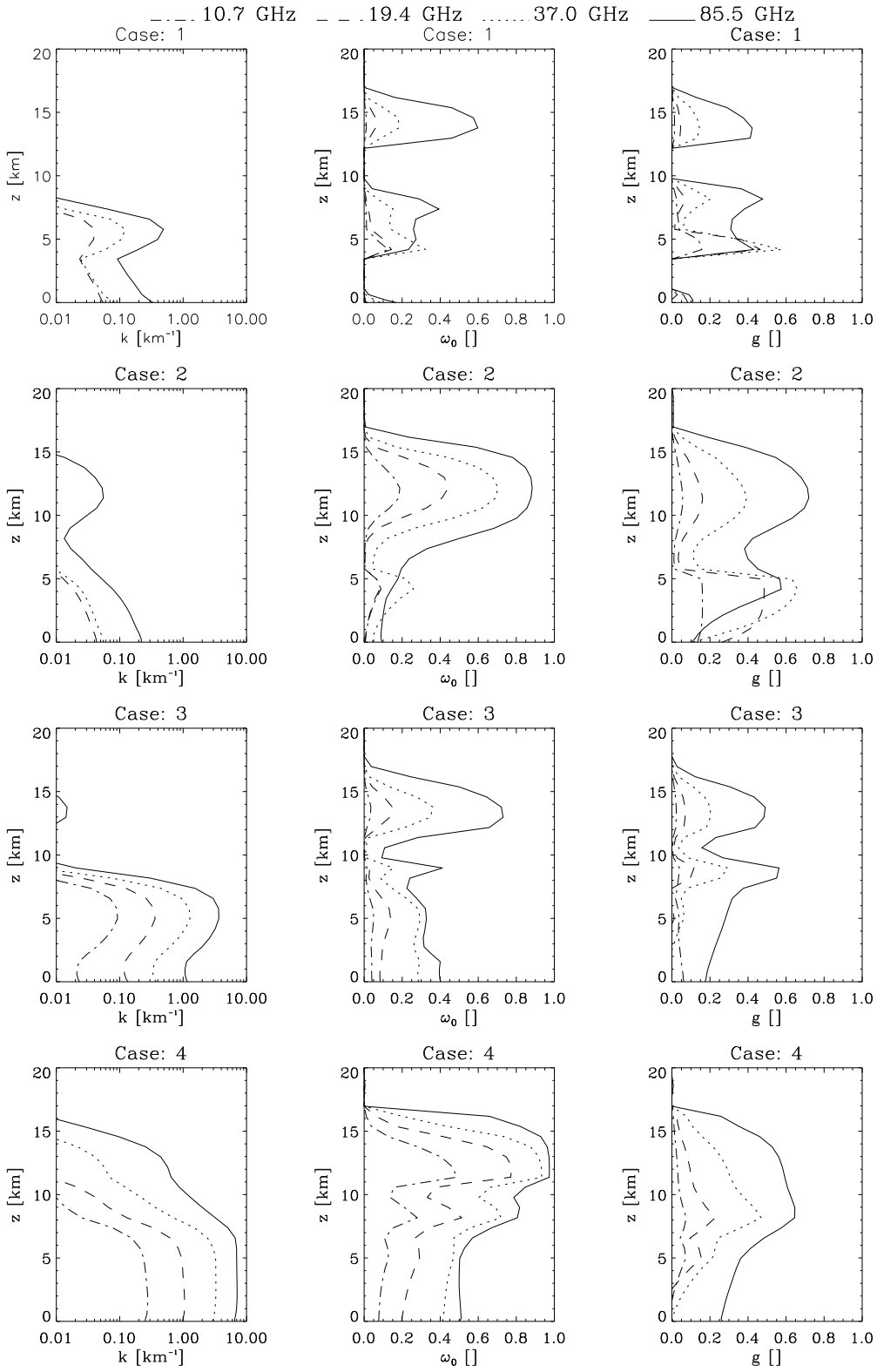

Figure 9: Profiles of optical parameters for four cases (rows) and the corresponding extinction coefficients, k, single scattering albedos, ω_o, and asymmetry parameters, g, at 4 microwave frequencies (columns).

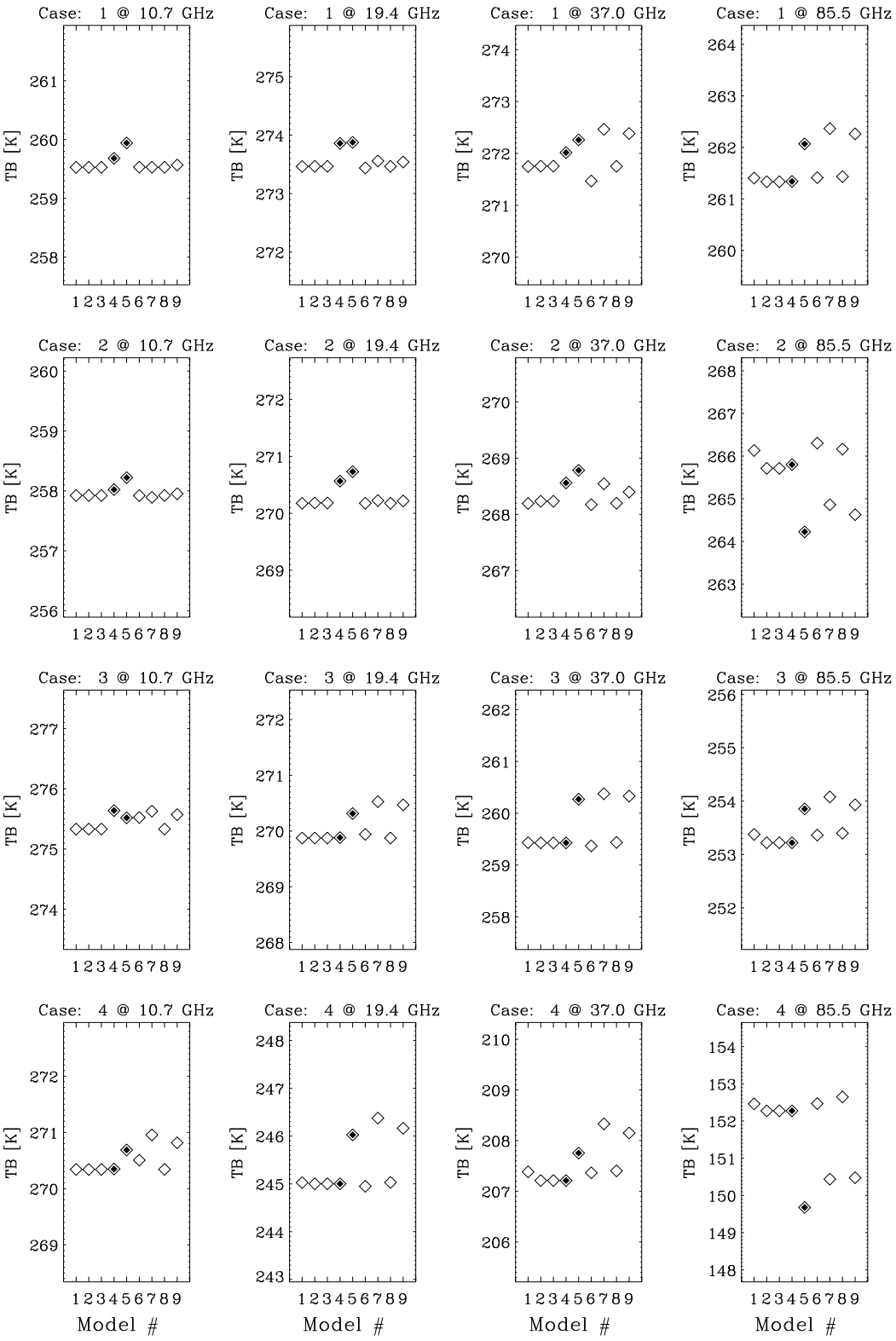

Figure 10: TB's at 53.1 degree incidence over land surface for four cases (rows) and at 10.7, 19.4, 37.0, and 85.5 GHz (columns); filled symbols mark models which assume Lambertian surface reflection.

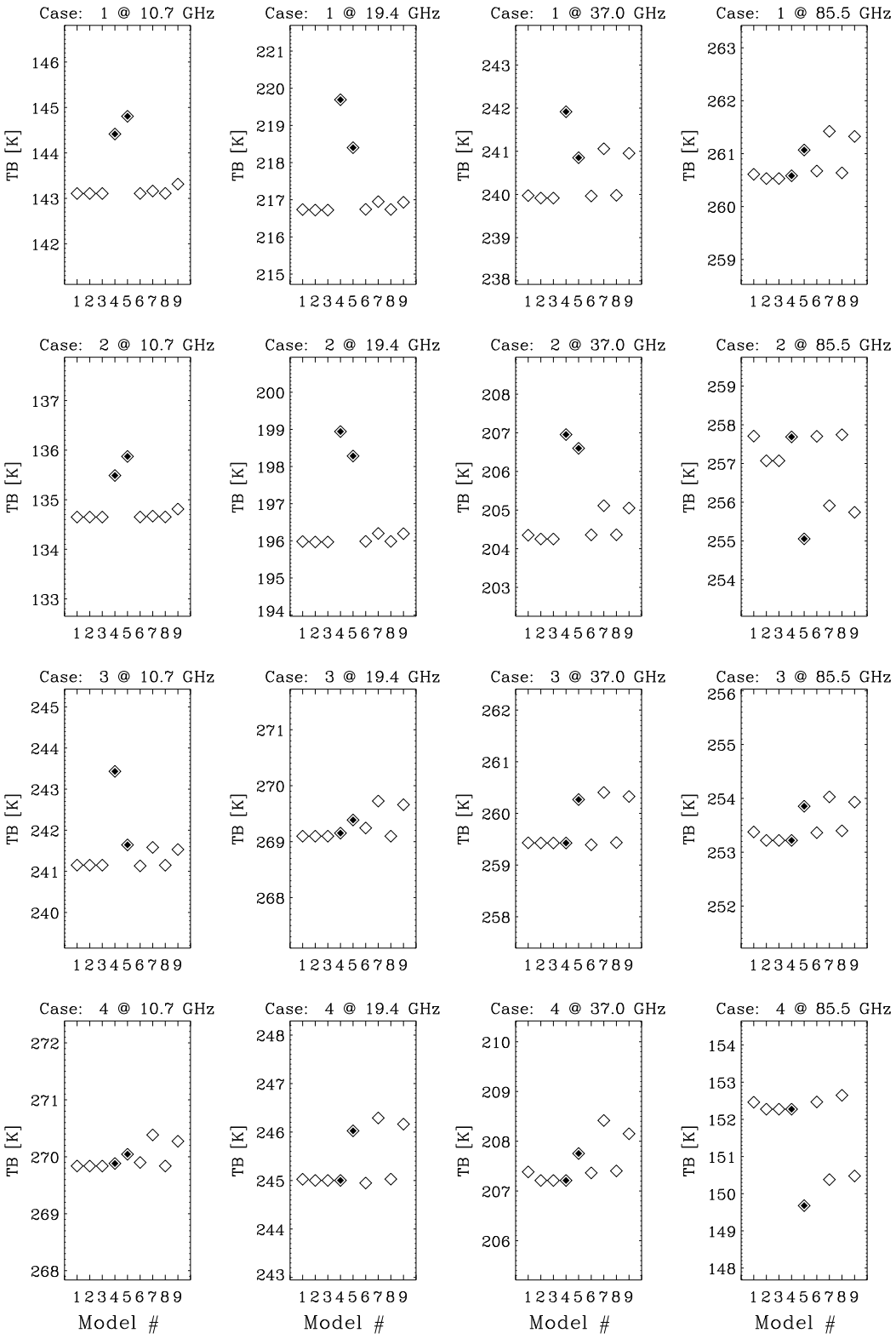

Figure 11: Same as Figure 10 for an ocean surface.